Lifshitz and other transitions in alkaline-earth 122 pnictides under pressure

Khandker Quader
Department of Physics, Kent State University, Kent, Ohio 44242, USA

Michael Widom
Department of Physics, Carnegie-Mellon University, Pittsburgh, Pennsylvania 15213, USA

(Received 28 January 2014; revised manuscript received 2 October 2014; published 21 October 2014; corrected 29 October 2014)

We carry out $T = 0$ first-principles total energy calculations in the entire set of alkaline 122-pnictides ($A\mathrm{Fe_2As_2}$; A = alkaline-earth element Ca, Sr, Ba, Ra) as a function of hydrostatic pressure. We find multiple distinct transitions to occur, namely an enthalpic transition in which the zero-pressure striped antiferromagnetic orthorhombic (OR-AFM) phase becomes thermodynamically less stable than a competing tetragonal (T) phase, a magnetic transition in which the OR-AFM phase loses its magnetism and orthorhombicity, and a lattice parameter anomaly in which the tetragonal c-axis collapses and a collapsed tetragonal (cT) phase becomes stable. Our results for energy band dispersions and spectra, lattice parameters, enthalpies, magnetism, and elastic constants over a wide range of hydrostatic pressure provide a coherent understanding of these experimentally observed transitions. In particular, the T-cT transition and anomalies in lattice parameters and elastic properties, observed at finite temperatures, are interpreted as arising from proximity to $T = 0$ Lifshitz transitions, wherein pressure causes nontrivial changes in the Fermi surface topology in these materials.

DOI: 10.1103/PhysRevB.90.144512 PACS number(s): 74.70.Xa, 74.62.Fj, 74.20.Pq

I. INTRODUCTION

Lifshitz transitions (LTs) [1], topological changes of a material's Fermi surface caused by external pressure or chemical substitution, are of considerable current interest. Changes in electronic band structure, such as disruption or creation of a Fermi surface neck, and creation or disappearance of a pocket, constitute typical topological changes. Because they require band dispersion extrema, LTs often appear on points or lines of high symmetry in the Brillouin zone. They are generally correlated with a van Hove singularity crossing the Fermi level, though this may not be straightforward to ascertain in nonelemental systems with complicated densities of states. At zero temperature, $T = 0$, LTs are true phase transitions of order 2 1/2 (as in Ehrenfest's classification), while at finite T, thermal smearing of the Fermi surface causes rapidly varying but analytic crossovers of properties [2]. Resulting anomalies in lattice parameters, density of states near the Fermi energy E_F, elastic properties, and electron dynamics manifest in observable thermodynamic and transport properties [1,2]. Present-day angle resolved photoemission spectroscopy (ARPES) experiments are capable of mapping Fermi surface topology, and thus can provide a more direct signature of LTs.

Of late, there has been interest in exploring possible effects of LTs in the iron arsenic compounds. The 122 pnictides, $A\mathrm{Fe_2As_2}$ (A = Ca, Sr, Ba), display structural, magnetic or superconducting phase transitions upon doping or applied pressure [3–6]; notably, a tetragonal phase (T) with a large c axis, "collapses" to a phase (cT) with a smaller c axis. Both tetragonal phases share the space group $I4/mmm$.

In this paper, based on $T = 0$ first-principles total energy density functional theory (DFT) calculations as a function of pressure, we obtain a number of results that are universal to all the alkaline-earth 122 pnictides. In particular, we propose that the T-cT transition observed at finite temperature actually results from a $T = 0$ Lifshitz transition in these 122-compounds. While at present there are no claims of observation of LTs in the pnictides under external pressure, recent ARPES experiments and theoretical interpretation provide evidence for LTs in doped Ba-122 [7,8], and interesting changes in electronic structure in Ca-122 [9] subjected to internal strain. Our results for energy band dispersions and spectra, c- and a-axis lattice parameters, magnetism, and elastic constants over a wide range of hydrostatic pressure, $P = 0$ to 60 GPa, enable us to provide a comprehensive understanding of the 122-pnictides under pressure. We include in our results, A = Ra, as it clarifies trends in behavior of the 122 series.

In the past, theoretical evidence for LTs under pressure have been found, for example, in DFT calculations of Zn and Cd [10] and Os [11]. Effects of LTs on thermodynamic and transport properties may be small and hence pose challenges for experimentalists. Nevertheless, LTs have been deduced, for example, from pressure study of elastic constants in $\mathrm{YCo_5}$ [12], Shubnikov-dHvA effect in Cd [13], and through the superconducting transition temperature (T_c) and magnetothermopower in Al [14].

The 122 pnictides share common structures (Fig. 1). At ambient pressure, Ca-, Sr-, Ba-122 compounds exhibit transitions from the high-temperature tetragonal (T) phase to a low temperature orthorhombic (OR) phase (space group Fmmm), striped along the a axis and antiferromagnetically (AFM) ordered along the c axis, at $T_{\mathrm{OR}} \sim 170$, 205, and 140 K, respectively [15–17]. This may be viewed as a magnetostructural transition from a high-T phase with fluctuating magnetic moments [18] to one with long-range AFM order. The T-OR transition temperature T_{OR} decreases with applied pressure.

Under hydrostatic pressure, at low-T, the 122-pnictides lose their OR-AFM state. Ca-122 and Sr-122 exhibit first-order transitions to the collapsed tetragonal (cT) phase with decreased c-axis value, at $P \sim 0.35$ GPa [19], and uncollapsed tetragonal (T) phase at $P \sim 4.4$ GPa [20,21], respectively. Ba-122 appears to undergo a continuous (or weakly first-order) transition at $P \sim 10.5$ GPa [22–24] to a T phase; experiments are variously at $T \sim 33$ and 100 K. The critical

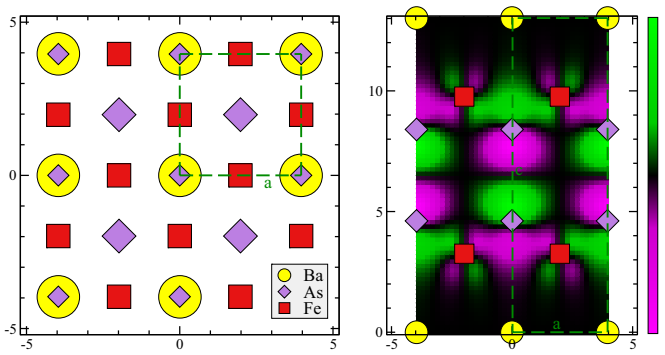

FIG. 1. (Color online) Lattice structure of 122 pnictides. The 122 pnictides AFe_2As_2 (A = Ca, Sr, Ba) possess the same lattice structures. (left) Structure of Ba-122 tetragonal (T) phase viewed along the (001) axis, from $z = 0$ to $c/2$. xy coordinates are given in units of Å. Atom size indicates z position, with large below small. (right) Structure within the xz plane at $y = 0$. Atoms are color-coded as on left. Background illustrates a purely real X-point wave function (see text), with scale bar linear in value.

pressures tend to be lower under nonhydrostatic conditions. With increased pressure, the T phase a- and c-axis parameters decrease smoothly until pressures, $P \sim 7$–10 GPa [20,25,26] and 29 GPa [22,27], respectively for Sr-122 and Ba-122, at which they evolve anomalously until the cT state is reached. High pressure x-ray diffraction studies of the Ba-122 and Sr-122 compounds attributed [26,27] these lattice parameter anomalies to a negative compressibility along the a axis.

Previous DFT calculations [28–30] have considered pressure and doping dependences. For Ba-122, two pressure-driven transitions were obtained, and abrupt jumps in the bulk modulus reported [29] at both low and high pressure transitions. A DFT-based molecular dynamics calculation [31] obtained two pressure-driven transitions in Ba-122 at low T. At higher T, the sharp OR-T transition at $P \sim 12.5$ GPa is shifted up to 15 GPa, and somewhat smoothed out, and at higher pressure the T-cT transition becomes almost indiscernible. It has been suggested [32] that reduction in c-axis parameter of Ca-122 under pressure results from increased As-As bonding caused by reduction of the Fe-magnetic moment. For Ba-122, collapse was similarly attributed to formation of an As-As bond [30]. As detailed below in Sec. IV, our model differs from both in that we focus on the elimination of an As-As *anti*bond. There has also been a study [33] that suggests that the cT phase transition in Ca- and Ba-122 can be understood within a Hund's rule correlation picture.

Our DFT total energy study systematically explores the different pressure-driven transitions in the entire alkaline-earth 122-pnictide family. We begin with the T and OR-AFM states at $P = 0$ and steadily increment the pressure, relaxing the structure at each P, and recording the equilibrium lattice parameters, total energy and magnetic moment. To explore dependence on the alkaline-earth element A, in addition to Ca-, Sr-, and Ba-122 pnictides, we also performed DFT calculations on $RaFe_2As_2$ and $MgFe_2As_2$ and compared their enthalpies to the pure elements and known stable binary phases. $MgFe_2As_2$ is found to be energetically unfavorable, both in its tI10 and oF20 forms. However, we predict that $RaFe_2As_2$, which may not be feasible to synthesize, is stable, and its pressure-driven transitions closely resemble those of Ba-122. We include this in our results as it clarifies trends in behavior of the 122 series.

II. METHOD

Our calculation utilizes the plane-wave based DFT code VASP [34] with the all-electron projector augmented wave method [35] carried out in the Perdew-Burke-Ernzerhof generalized gradient approximation [36] to the exchange-correlation potential. Calculations are performed within the unit cells with Pearson type tI10 for the tetragonal phase and oF20 for the orthorhombic phase. However, a $\sqrt{2}\times\sqrt{2}$ supercell of tI10 is employed for consistency with oF20 for calculations of ΔH. Striped antiferromagnetic collinear spin configurations are utilized in the OR-AFM state.

Energy cutoffs and k-point meshes are increased to converge total energies to better than 1 meV/atom. In particular, we utilized a plane wave energy cutoff of 320 eV for all calculations reported, which exceeds the default cutoff for Fe by 20%. We employed k-point meshes ranging from $8\times8\times4$ for oF20 unit cells up to $11\times11\times5$ for tI10 unit cells and $11\times11\times11$ for tI10 primitive cells. Special k points utilized in band structures are [37] $\Gamma = (0,0,0)$, $X = (0,0,1/2)$, $M = Z' = (-1/2,1/2,1/2)$, and $Z = (1/2,1/2,-1/2)$ in reciprocal coordinates. All calculations were performed using the VASP setting PREC=Accurate so as to avoid Fourier transform wrap-around errors. Fermi surface smearing of 0.2 eV is employed for relaxations and 0.05 eV for ΔH values. Precise transition pressures were found to be sensitive to smearing, but we did not attempt to converge in this variable. Densities of states utilize tetrahedron integration with subsequent Gaussian smearing of 0.01 eV. Elastic constants were calculated within VASP by finite differences of stress with respect to strain.

To observe pressure-driven transitions, we begin with $P = 0$ structures and increase the pressure in steps of 1 GPa (0.5 GPa for the case of Ca-122), fully relaxing the lattice parameters and internal coordinates at each step until the maximum force is less than 0.01 eV/Å. Accurate values for P_H and P_L were obtained by linear interpolation to locate $\Delta H = 0$ (for P_H) and $E(k) = E_F$ (for P_L), while steps as low as 0.1 GPa were utilized to resolve P_M.

III. CALCULATED TRANSITIONS UNDER PRESSURE

Our key results are summarized in Fig. 2 and Table I. We find three types of transition to occur: an enthalpic transition, in which the OR-AFM state loses thermodynamic stability to a tetragonal state; a magnetic transition, in which the OR-AFM state loses its magnetic moment; a transition in which the tetragonal T state collapses to cT, identified as the Lifshitz transition; see Sec. IV. These transitions occur in different sequences depending on A; hence some occur within metastable states and will not be observed in experiments in thermodynamic equilibrium.

A. Enthalpic transition at P_H

This is shown in Fig. 2(a). For A = Ca, both OR-AFM and nonmagnetic states exist simultaneously at pressures above and below P_H. However, high-P favors the lower volume cT state causing the enthalpy difference $\Delta H \equiv H_{cT} - H_{OR} = \Delta E - P\Delta V$ to change sign at P_H [38]. The situation is similar

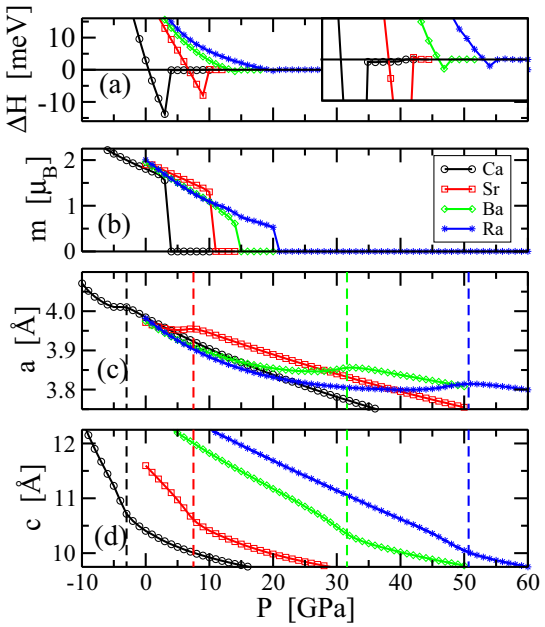

FIG. 2. (Color online) Key pressure-dependent results for A-122 pnictides, A = Ca, Sr, Ba, and Ra. (a) Enthalpy differences $\Delta H = H_{\rm cT} - H_{\rm OR}$ between tetragonal and OR-AFM phases; the inset enlarges the $\Delta H = 0$ crossings. (b) Magnetic moments vanishing abruptly at the magnetic transition P_M. (c) and (d) show the anomalous behavior of the tetragonal a and c axis parameters. Vertical dashed lines indicate T-cT transition (identified as the Lifshitz transition) pressures, P_L.

for A = Sr, Ba, Ra, with the exception that the transition from OR-AFM is to an *uncollapsed* tetragonal state T, rather than the collapsed cT. For all A, the OR-AFM state continues as a metastable state for $P > P_H$ and no magnetic or lattice anomalies occur upon crossing P_H. P_H is progressively larger for A = Ca, Sr, Ba, Ra because ΔE is greater, and the volume difference ΔV is smaller. Because ΔH crosses zero linearly at P_H, these transitions are *first order* for all four 122 pnictides considered here, although in the case of Ba and Ra the transition is nearly continuous (i.e., weakly first order).

B. Magnetic transition at P_M

For all four 122 compounds, the magnetic moments vanish suddenly, i.e., no stable OR-AFM state exists for $P > P_M$, even though it exists and maintains a large magnetic moment for $P_H < P < P_M$; see Fig. 2(b). Note the strict inequality

TABLE I. Calculated critical pressures for $T = 0$ transitions common to the 122 pnictides. All pressures are in GPa. P_H denotes enthalpic transition, in which the OR-AFM state loses thermodynamic stability to a tetragonal state. P_M is the magnetic transition at which the OR-AFM state loses its magnetic moment ($M = 0$). P_L is identified as a Lifshitz transition.

A	P_H	P_M	P_L
Ca	0.46	3.2	−3.2
Sr	6.7	9.3	7.5
Ba	13.3	14.6	32
Ra	19.2	20.4	51

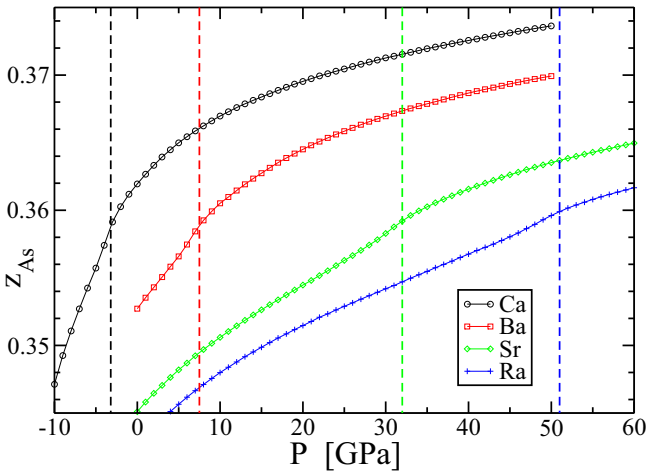

FIG. 3. (Color online) Optimal As z coordinate vs pressure. Dashed lines indicate P_L for each compound.

$P_H < P_M$ owing to the metastable (*i.e.* mechanically stable but enthalpically unfavorable) extension of the OR-AFM state, a distinction not widely recognized [29,30]. Thus for Ca-122 and Ba-122, P_c and P_{c1}, respectively [29], correspond to our P_M; not distinguishing this from P_H can lead to a large error in estimating the critical pressure for Ca-122. Distinguishing P_H from P_M allows us to recognize that though a striped-AFM state exists for $P_H < P < P_M$, it is not stable for $P > P_M$, in contrast with previous work [30]. The existence of the metastable state is verified by the experimental observation of hysterisis in the case of Ca-122 [39].

C. Collapsed tetragonal phase: characteristic pressure P_L

In our picture, P_L separates the two tetragonal states, T and cT. Figures 2(c) and 2(d) shows that for all four 122 pnictides, P_L is characterized by anomalies in tetragonal a and c axis lattice parameters. The a axis varies nonmonotonically, and c axis shows an inflection, although the unit cell volume $V = a^2c$ decreases monotonically with P as required by thermodynamics. P_L increases monotonically with A as it advances down the periodic table. For A = Ca, we find the anomalies in a and c occur at a negative pressure, $P_L = -3.2$ GPa, and hence the transition at $P_H = 0.46$ GPa goes directly from OR to cT. The transitions are fully reversible, as the lattice parameter curves exactly reproduce without hysteresis under increasing or decreasing pressure.

We have checked the behavior of internal coordinates with pressure as well. The tetragonal crystal structure contains a single internal parameter, the As z parameter that governs the As-As interatomic spacing. This quantity evolves monotonically with pressure P, and displays only a weak inflection in the vicinity of P_L as can be seen in Fig. 3.

Our calculated transition pressures for the enthalpic (P_H), magnetic (P_M), and T-cT (P_L) transitions for AFe$_2$As$_2$ (A = Ca, Sr, Ba, Ra) are given in Table I.

IV. T-cT TRANSITION DRIVEN BY LIFSHITZ TRANSITION

We have discussed in Sec. III C that, for each of the 122-pnictides, a characteristic pressure, P_L can be associated

with the anomalous behavior in the tetragonal a and c lattice parameters, and the T-cT transition; see Figs. 2(c) and 2(d). Below, we show that our calculations of electronic structure, elastic constants, and bond lengths, for different pressures, in the 122 pnictides, provide support to our claim that the T-cT transition arises from a Lifshitz transition.

A. Electronic structure

Our electronic structure calculations give *band dispersions* along different k-directions, and also the density of states (DOS) integrated over the full Brillouin zone. Since the results are similar overall for all 122 pnictides, as a prototypical case, we discuss in details the Ba-122 compound; selected band structure for the other 122 compounds shown later.

Figure 4 shows the dispersion relations for individual bands for Ba-122 at representative pressures (see Appendix for other A-122's). We draw particular attention to the band at the X point, comprised mostly of anti-bonding As-p_z, mixed with bonding Fe-$d_{xz,yz}$ orbitals (see wave function in Fig. 1). As Fig. 4(b) shows, this band lies below E_F at $P = 28$ GPa, forming an electron pocket, while Fig. 4(c) shows that at

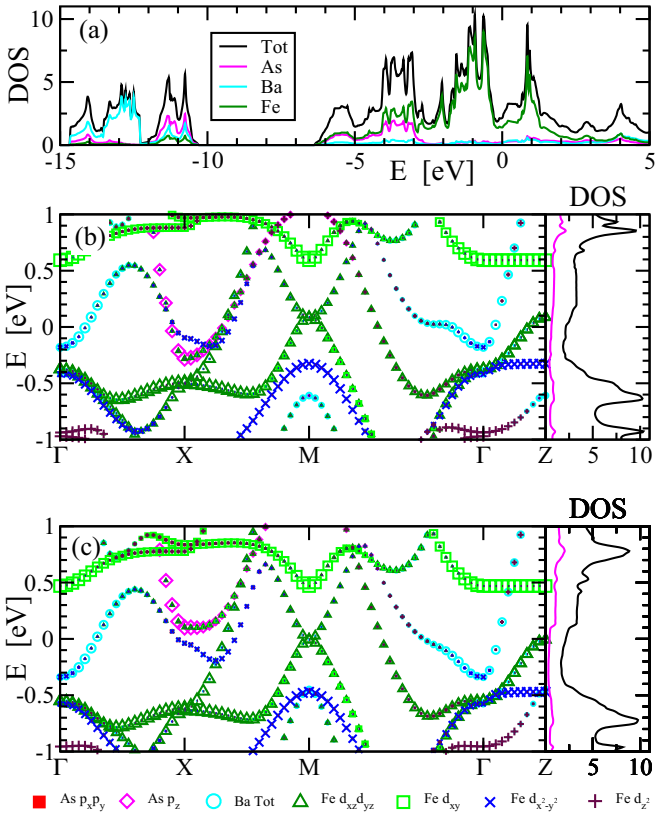

FIG. 4. (Color online) Band structure and density of states (DOS) for Ba-122 (a) Total density of states (DOS) and Fe, As, and Ba partial DOS over a wide range of energy at $P = 28$ GPa. (b) and (c) Band structures in the primitive tetragonal cell Brillouin zone [29,37] at $P = 28$ and 34 GPa, i.e., below and above P_L, respectively. The corresponding total and As partial DOS around E_F are shown alongside; the As DOS has been scaled 3x to make it more visible. Note that the As p_z electron pocket at the X point moves above E_F for $P > P_L$. Plotting symbol size indicates the projection onto atomic orbitals.

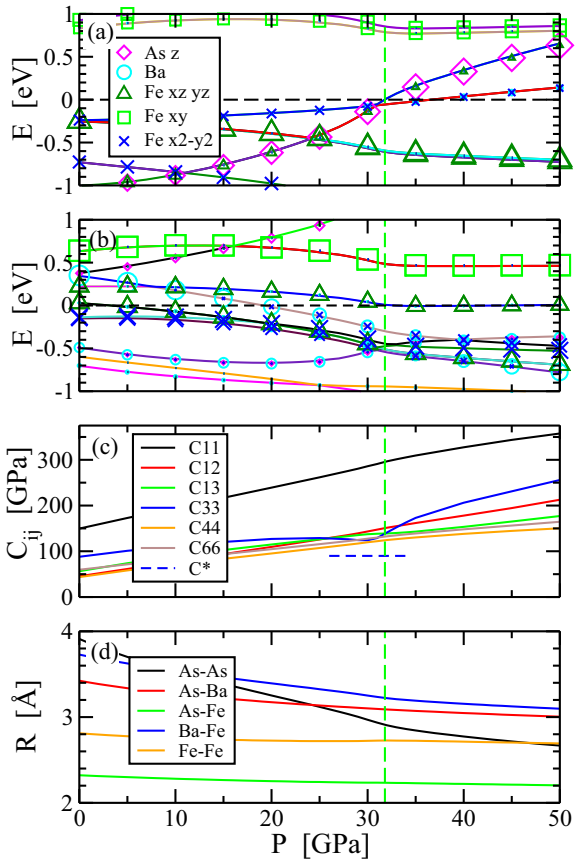

FIG. 5. (Color online) Pressure variations of key quantities for Ba-122. (a) X-point bands; (b) M- and Γ-point bands. Dashed vertical line locates P_L. (c) Tetragonal elastic constants calculated within VASP. The dashed horizontal line indicates the limit for elastic stability (see text). (d) Interatomic separations.

$P = 34$ GPa, this band has moved to above E_F, so that the electron pocket has emptied; the transition occurs at $P_L = 31.6$ GPa.

Pressure dependence of this and other bands are illustrated Figs. 5(a) and 5(b). This topological change in the Fermi surface correlates strongly with the anomalous behavior of the a and c lattice parameters discussed above and shown in Fig. 2. We take this X-point band crossing to define the value of P_L, which we recognize as a Lifshitz transition. This corresponds to a van Hove singularity in DOS that moves across E_F, and can be seen most clearly above P_L in Fig. 4(c). Additional bands can be seen crossing E_F in Figs. 5(a) and 5(b) indicating that other Lifshitz transitions exist, which is not surprising given the large number of bands in a crystal structure with many atoms per unit cell.

We point out an unusual feature at the M point (note that $M = Z'$ owing to body centering [29]): a set of degenerate bands, dominated by Fe-$d_{xz,yz}$ antibonding [30] orbitals, move from above E_F for $P = 28$ GPa [Fig. 4(b)] to below E_F for $P > 33$ GPa [Fig. 4(c)], reaching a minimum value of only 7 meV below E_F, then drifting very slowly back up with further increase of pressure. Additional studies with stricter convergence confirm that the band is not pinned at E_F. Furthermore, the same state is pinned distinctly below

E_F in the case of Ra-122, and the band-structure topology differs in the cases of Ca- and Sr-122 (see Appendix). Hence we believe this state has no relevance to the T-cT transition.

B. Elastic constants and bond lengths

The elasticity tensor for tetragonal symmetry in Voigt notation is

$$\mathbf{C} = \begin{pmatrix} C_{11} & C_{12} & C_{13} & 0 & 0 & 0 \\ C_{12} & C_{11} & C_{13} & 0 & 0 & 0 \\ C_{13} & C_{13} & C_{33} & 0 & 0 & 0 \\ 0 & 0 & 0 & C_{44} & 0 & 0 \\ 0 & 0 & 0 & 0 & C_{44} & 0 \\ 0 & 0 & 0 & 0 & 0 & C_{66} \end{pmatrix}. \quad (1)$$

Elastic stability requires this tensor to be positive definite [40]. The eigenvalues are

$$\begin{aligned} \lambda_1 &= C_{11} - C_{12}, \\ \lambda_{2,3} &= \tfrac{1}{2}\left[C_{11} + C_{12} + C_{33}, \ \pm\sqrt{8C_{13}^2 + (C_{33} - C_{11} - C_{12})^2}\right], \\ \lambda_{4,5} &= C_{44}, \\ \lambda_6 &= C_{66}. \end{aligned} \quad (2)$$

Both λ_2 and λ_3 vanish when $C_{33} = 2C_{13}^2/(C_{11} + C_{12})$.

Figure 5(c) shows the variation of the calculated tetragonal elastic constants with pressure. While most elastic constants increase monotonically with pressure, C_{33}, related to stress strain along the c axis, displays anomalous behavior around the T-cT Lifshitz transition pressure, P_L. Slightly below P_L, C_{33} decreases with pressure to a minimum, and then increases again beyond P_L. As can be seen, C_{33} lies above the limit of elastic stability [40], i.e., $C_{33} > C^* = 2C_{13}^2/(C_{11} + C_{12}) =$ 86 GPa, given the values of C_{ij} at P_L. Evidently, the T phase is heading towards an elastic instability in the vicinity of P_L that is avoided by the transition into the cT state. We note that C_{33}, and hence compressibility, does not go negative, contrary to some views in literature [26,27].

Figure 5(d) shows the behavior of various calculated bond lengths with pressure. The As-As bond length drops below 3 Å, reaching 2.9 Å as $P \to P_L$. As we discussed above, the X-point band that crosses E_F at P_L is dominated by As-p_z orbitals between As atoms that are neighbors in the z direction, and hence their separation closely tracks the variation of the c axis. As the As-As bond length drops, causing the energy of this repulsive antibond [shown in Fig. 1(b)] to rise towards E_F, the resulting depletion of the repulsive bond softens C_{33}. Following the collapse, other repulsive forces stabilize the structure with a reduced c axis, as can be seen in the subsequent rise of C_{33}. The same wave function is bonding between As and Fe [Fig. 1(b)], so its depletion can be associated with the increase in the a lattice parameter. Presumably the value of P_L grows with increasing atomic radius of the alkali-earth element because greater pressure is required to drive the As–As bond length below 3 Å.

V. DISCUSSION

Previous work [30] on the electronic origin of the T-cT transition in Ba-122 attributes the transition with a band touching at Z' associated with a covalent As-As interlayer bond. Note that Z' is identical to our M point, and this band touching is thus the "unusual feature" described in Section IV A that has no significance for the T-cT transition. Rather, in our model T-cT is primarily driven by the crossing at the X point leading to the loss of the interlayer As antibonding state. Similar band structure and bonding characteristics are present in other compounds such as $SrRh_2P_2$, with P playing the role of As [41,42].

Our calculations show that the alkaline-earth 122 pnictides, under pressure, exhibit several features, which are universal within this family. One key result is that at high pressures

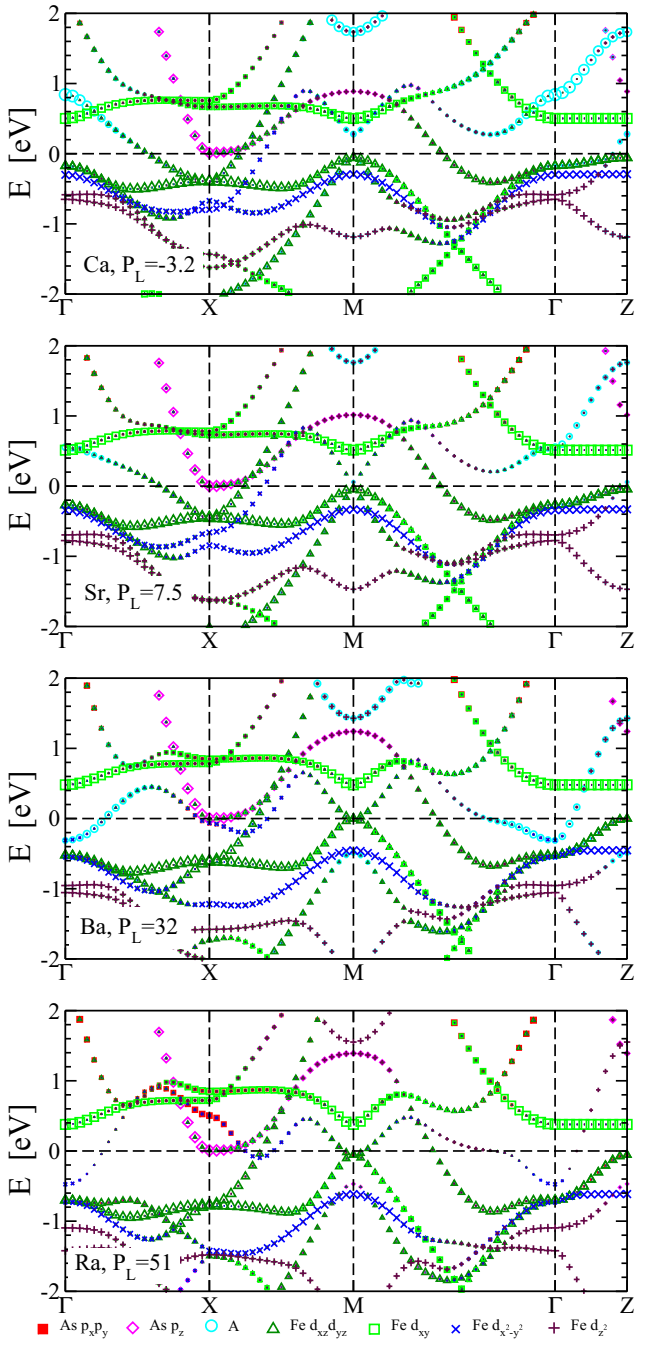

FIG. 6. (Color online) Band structures of tetragonal A-Fe_2As_2 with (top to bottom) A = Ca, Sr, Ba, Ra, at pressure $P_L = -3.2, 7.5,$ 32, and 51 GPa, respectively.

these pnictides exhibit Lifshitz transitions characterized by the vanishing of an electron pocket at the X point, as it moves from below to above the Fermi energy. This correlates well with anomalies in lattice parameters and elastic constants around the Lifshitz transition pressure, P_L. We suggest that the finite-temperature T-cT transitions, which occur in all the 122 compounds, are consequences of the $T = 0$ Lifshitz transitions. This provides a novel explanation for the observed anomalies in lattice parameters and elastic constants, and one that is different from those existent in literature. At finite T, the Lifshitz transition normally becomes a smooth crossover, but could conceivably be driven first order through lattice phonons and/or spin fluctuations. We also find additional Lifshitz transitions at other pressures. At lower pressures, P_H, these 122 pnictides all undergo first-order enthalpic transitions from a AFM-OR phases to nonmagnetic T or a cT phases. In all cases, metastable magnetic OR phases persist up to higher pressures, P_M, when magnetism is lost by first-order transitions. Our calculations are consistent with a large number of experimental observations by different groups.

ACKNOWLEDGMENTS

We thank Karin Rabe, Di Xiao, Leon Balents, Paul Canfield and Alan Goldman for useful discussions. We acknowledge the hospitality of Aspen Center for Physics, where part of the manuscript was written.

APPENDIX

Our calculated band structures of all the tetragonal A-Fe_2As_2 (A = Ca, Sr, Ba, Ra) 122-compounds at their respective Lifshitz transition pressures are shown in Fig. 6. The common features of Lifshitz transition at the T-cT transition at pressure $P_L = -3.2, 7.5, 32$, and 51 GPa, respectively, are evident here. As for Ba-122, we find a similar degenerate band-pinning for Ra-122 slightly below E_F, converting a hole pocket into a very small electron pocket, as can be seen in the figure. Note different band topologies obtained for Ca-122 and Sr-122.

[1] I. M. Lifshitz, Sov. Phys. JETP **11**, 1130 (1960).

[2] A. Varlamov, V. Edorov, and A. Pantsulaya, Adv. Phys. **38**, 469 (1989).

[3] P. Alireza, Y. T. Ko, J. Gillett, C. M. Petrone, J. M. Cole, G. G. Lonzarich, and S. E. Sebastian, J. Phys.: Condens. Matter **21**, 012208 (2009).

[4] M. S. Torikachvili, S. L. Bud'ko, N. Ni, P. C. Canfield, and S. T. Hannahs, Phys. Rev. B **80**, 014521 (2009).

[5] A. Mani, S. Ghost, S. Paulraj, A. Bharathi, and C. S. Sundar, Europhys. Lett. **87**, 17004 (2009).

[6] S. R. Saha, N. P. Butch, T. Drye, J. Magill, S. Ziemak, K. Kirshenbaum, P. Y. Zavalij, J. W. Lynn, and J. Paglione, Phys. Rev. B **85**, 024525 (2012).

[7] C. Liu, T. Kondo, R. M. Fernandes, A. D. Palczewski, E. D. Mun, N. A. Ni, A. N. Thaler, A. Bostwick, E. Rotenberg, J. Schmalian, S. L. Bud'ko, P. C. Canfield, and A. Kaminski, Nat. Phys. **6**, 419 (2010).

[8] C. Liu, A. D. Palczewski, R. S. Dhaka, T. Kondo, R. M. Fernandes, E. D. Mun, H. Hodovanets, A. N. Thaler, J. Schmalian, S. L. Bud'ko, P. C. Canfield, and A. Kaminski, Phys. Rev. B **84**, 020509 (2011).

[9] R. S. Dhaka, R. Jiang, S. Ran, S. L. Bud'ko, P. C. Canfield, B. N. Harmon, A. Kaminski, M. Tomić, R. Valentí, and Y. Lee, Phys. Rev. B **89**, 020511(R) (2014).

[10] D. L. Novikov, M. I. Katsnelson, A. V. Trefilov, A. J. Freeman, N. E. Christensen, A. Svane, and C. O. Rodriguez, Phys. Rev. B **59**, 4557 (1999).

[11] D. Koudela, M. Richter, A. Möbius, K. Koepernik, and H. Eschrig, Phys. Rev. B **74**, 214103 (2006).

[12] H. Rosner, D. Koudela, U. Schwarz, A. Handstein, M. Hanfland, I. Opahle, K. Koepernik, M. D. Kuz'min, K.-H. Müller, J. A. Mydosh, and M. Richter, Nat. Phys. **2**, 469 (2006).

[13] S. L. Bud'ko, A. N. Voronovskii, A. G. Gapotchenko, and E. S. ltskevich, Zh. Eksp. Teor. Fiz. **86**, 778 (1984) [Sov. Phys. JETP **59**, 454 (1984)].

[14] D. R. Overcash, T. Davis, J. W. Cook, and M. J. Skove, Phys. Rev. Lett. **46**, 287 (1981).

[15] M. S. Torikachvili, S. L. Bud'ko, N. Ni, and P. C. Canfield, Phys. Rev. B **78**, 104527 (2008).

[16] C. Krellner, N. Caroca-Canales, A. Jesche, H. Rosner, A. Ormeci, and C. Geibel, Phys. Rev. B **78**, 100504 (2008).

[17] Q. Huang, Y. Qiu, W. Bao, M. A. Green, J. W. Lynn, Y. C. Gasparovic, T. Wu, G. Wu, and X. H. Chen, Phys. Rev. Lett. **101**, 257003 (2008).

[18] S. O. Diallo, D. K. Pratt, R. M. Fernandes, W. Tian, J. L. Zarestky, M. Lumsden, T. G. Perring, C. L. Broholm, N. Ni, S. L. Bud'ko, P. C. Canfield, H.-F. Li, D. Vaknin, A. Kreyssig, A. I. Goldman, and R. J. McQueeney, Phys. Rev. B **81**, 214407 (2010).

[19] P. Canfield, S. Budko, N. Ni, A. Kreyssig, A. Goldman, R. McQueeney, M. Torikachvili, D. Argyriou, G. Luke, and W. Yu, Physica C **469**, 404 (2009).

[20] S. Ikeda, K. Yoshida, and H. Kobayashi, Hyperfine Interact. **208**, 7 (2012).

[21] H. Kotegawa, T. Kawazoe, H. Sugawara, K. Murata, and H. Tou, J. Phys. Soc. Jpn. **78**, 083702 (2009).

[22] R. Mittal, S. K. Mishra, S. L. Chaplot, S. V. Ovsyannikov, E. Greenberg, D. M. Trots, L. Dubrovinsky, Y. Su, T. Brueckel, S. Matsuishi, H. Hosono, and G. Garbarino, Phys. Rev. B **83**, 054503 (2011).

[23] W. J. Duncan, O. P. Welzel, C. Harrison, X. F. Wang, X. H. Chen, F. M. Grosche, and P. G. Niklowitz, J. Phys.: Condens. Matter **22**, 052201 (2010).

[24] T. Yamazaki, N. Takeshita, R. Kobayashi, H. Fukazawa, Y. Kohori, K. Kihou, C.-H. Lee, H. Kito, A. Iyo, and H. Eisaki, Phys. Rev. B **81**, 224511 (2010).

[25] D. Kasinathan, M. Schmitt, K. Koepernik, A. Ormeci, K. Meier, U. Schwarz, M. Hanfland, C. Geibel, Y. Grin, A. Leithe-Jasper, and H. Rosner, Phys. Rev. B **84**, 054509 (2011).

[26] W. O. Uhoya, J. M. Montgomery, G. M. Tsoi, Y. K. Vohra, M. A. McGuire, A. S. Sefat, B. C. Sales, and S. T. Weir, J. Phys.: Condens. Matter **23**, 122201 (2011).
[27] W. Uhoya, A. Stemshorn, G. Tsoi, Y. K. Vohra, A. S. Sefat, B. C. Sales, K. M. Hope, and S. T. Weir, Phys. Rev. B **82**, 144118 (2010).
[28] M. D. Johannes, I. I. Mazin, and D. S. Parker, Phys. Rev. B **82**, 024527 (2010).
[29] M. Tomic, R. Valenti, and H. O. Jeschke, Phys. Rev. B **85**, 094105 (2012).
[30] N. Colonna, G. Profeta, A. Continenza, and S. Massidda, Phys. Rev. B **83**, 094529 (2011).
[31] S. Backes and H. O. Jeschke, Phys. Rev. B **88**, 075111 (2013).
[32] T. Yildirim, Phys. Rev. Lett. **102**, 037003 (2009).
[33] W. Ji, X.-W. Yan, and Z.-Y. Lu, Phys. Rev. B **83**, 132504 (2011).
[34] G. Kresse and J. Furthmuller, Phys. Rev. B **54**, 11169 (1996).
[35] G. Kresse and D. Joubert, Phys. Rev. B **59**, 1758 (1999).
[36] J. P. Perdew, K. Burke, and M. Ernzerhof, Phys. Rev. Lett. **77**, 3865 (1996).
[37] O. K. Andersen and L. Boeri, Ann. Phys. **523**, 8 (2011).
[38] M. Widom and K. Quader, Phys. Rev. B **88**, 045117 (2013).
[39] A. I. Goldman, A. Kreyssig, K. Prokeš, D. K. Pratt, D. N. Argyriou, J. W. Lynn, S. Nandi, S. A. J. Kimber, Y. Chen, Y. B. Lee, G. Samolyuk, J. B. Leão, S. J. Poulton, S. L. Bud'ko, N. Ni, P. C. Canfield, B. N. Harmon, and R. J. McQueeney, Phys. Rev. B **79**, 024513 (2009).
[40] C. Kittel, *Introduction to Solid State Physics*, 8th ed. (Wiley, New Jersey, 2005).
[41] D. Johrendt, C. Felser, O. Jepsen, O. K. Andersen, A. Mewis, and J. Rouxel, J. Solid State Chem. **130**, 254 (1997).
[42] C. Huhnt, G. Michels, M. Roepke, W. Schlabitz, A. Wurth, D. Johrendt, and A. Mewis, Physica B **240**, 26 (1997).